Research Article Vol. 58, No. 34 / 1 December 2019 / Applied Optics G241

applied optics

Holographic amplification of the diffraction angle from optical phase array for optical beam steering

Colton M. Bigler,* Zachary Rovig, Joshua McDonald, and Pierre-Alexandre Blanche

James C. Wyant College of Optical Sciences, University of Arizona, 1630 E University Boulevard, Tucson, Arizona 85719, USA
**Corresponding author: cbigler@optics.arizona.edu*

Received 8 July 2019; revised 27 September 2019; accepted 8 October 2019; posted 8 October 2019 (Doc. ID 372007); published 6 November 2019

Beam steering in lidar applications presents an important engineering problem, as researchers seek to achieve the highest possible field of view with low energy cost and rapid refresh rate. Non-mechanical beam-steering technologies that exist today are known to achieve a low energy cost and rapid refresh rate, but they have a narrow angular range. A method by which the diffraction angle from a beam-steering device may be increased to cover a 4π sr solid angle is presented. Multiple holograms are recorded in the same volume hologram in a process called multiplexing. This multiplexed hologram can diffract light over a solid angle of 2π sr. To increase the angular coverage up to 4π sr, a hemispheric lens is attached to the volume hologram. Secondary holographic optical elements coated on the lens surface further diffract the light, directing it to a theoretical maximum of 4π sr. An early prototype demonstrates five distinct diffraction angles, ranging from 20° to 150°, which covers a solid angle around 90% of the entire sphere while maintaining beam collimation.

https://doi.org/10.1364/AO.58.00G241

1. INTRODUCTION

Light detection and ranging (lidar) is a technique typically used in remote sensing applications where pulsed laser light is shined on a target and the reflected pulses are measured by a sensor. Because of the delay between returned pulses, lidar allows users to generate a depth map of a scene. This makes it useful for remote sensing applications, such as self-driving cars [1].

Beam steering ensures the angular coverage of the lidar system. Approaches to beam steering generally fall into three categories: mechanical steering, micro-electro-mechanical systems (MEMS), and non-mechanical steering [2].

Mechanical steering refers to systems with physical optics that are rotated or positioned to steer the beam to the desired position. These systems include gimbals, fast-steering mirrors, wedge prism pairs, and rotating mirrors and gratings [3–5]. While they are very effective at directing the energy in the desired direction, mechanical steering solutions are hindered by their inertia and high energy cost. Additionally, many mechanical beam-steering systems have relatively greater size, weight, and cost than their non-mechanical or MEMS counterparts, as well as increased sensitivity to motion and vibration.

MEMS beam-steering efforts seek to accomplish beam steering with drastically lower inertia and power costs than their traditional mechanical counterparts [6–9]. Though there is actual mechanical movement with MEMS, the rotation is that of a collection of small mirrors rotated on an optical axis, which allows for small size and weight, in addition to the lower inertia and power costs previously discussed. These systems are limited, however, as there is a trade-off between the diffraction angle and the size of the beam that can be diffracted. Ongoing research efforts seek to expand the range of diffraction angles from a MEMS device while maintaining a large beam size [2].

Non-mechanical steering systems use phase control across diffractive surfaces to steer the beam into the desired direction [10–13]. Frequently, this steering is accomplished with a photonic chip, spatial light modulator (SLM), or digital micromirror device (DMD). While this configuration is quickly re-configurable and operates without the high inertia and energy cost of their mechanical counterparts, the limitation of these non-mechanical steering systems is that they have relatively narrow steering angles ($\approx 1°$) [10], as the light is diffracted according to Bragg's law [14]:

$$\sin\theta_B = m\frac{\lambda_0/n}{2\Lambda}, \tag{1}$$

where θ_B is the Bragg angle, m is the diffraction order, λ_0 is the vacuum wavelength, n is the refractive index, and Λ is the distance between Bragg planes. For instance, with the HOLOEYE LC-R720 SLM, which was used in the demonstrator discussed below, pixel pitch is 20 μm. For an example grating that repeats every four pixels, working at 532 nm in air, $\theta_B = 0.191°$ for the first diffraction order. Non-mechanical steering devices have

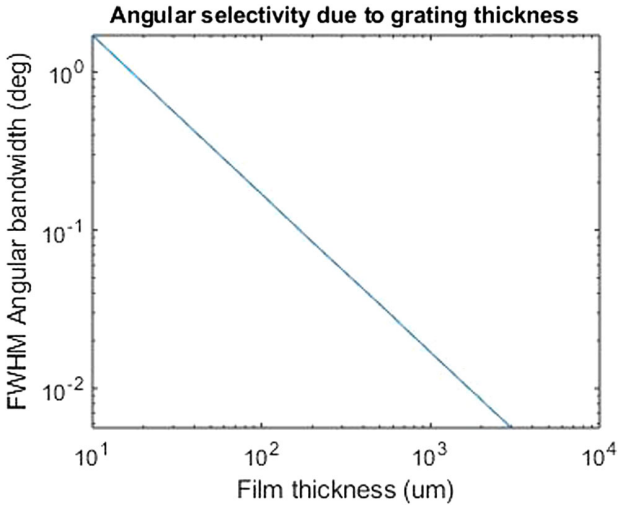

Fig. 1. Increasing the thickness of the holographic film increases the angular selectivity of the recorded holograms when paired with a proportional decrease in refractive index modulation. For angular selectivity less than 0.1°, the film thickness needs to be at least 200 μm.

great potential that is fundamentally limited by the range of angles over which such a device can steer incident light. Our angular amplification system seeks to unlock that potential for wide-angle, commercial, beam-steering applications by increasing the effective angular range of non-mechanical steering systems.

The system presented in this paper uses holograms to amplify the steering angle from a non-mechanical steering system to cover a solid angle of nearly 4π sr. A multiplexed, thick volume hologram diffracts incident light into a 2π sr hemisphere. The material characteristics of this hologram are chosen to minimize crosstalk between different gratings by increasing the angular selectivity of individual gratings. After interacting with the thick volume hologram, the diffracted light is incident on the hemispheric surface, which is coated with holograms to counteract the optical power of the hemisphere and further redirect the beams up to 4π sr. Angular selectivity is determined by the effective grating thickness and refractive index modulation of the substrate, as dictated by Kogelnik's coupled wave theory (CWT) [15,16]. Increasing the grating thickness while decreasing the refractive index modulation increases the angular selectivity of the material. For a transmission phase hologram, the dispersion equation of diffraction efficiency (DE) as a function of thickness is

$$\frac{d\eta_{\mathrm{TE}}}{dd} = 2\frac{\pi\Delta n}{\lambda\cos\theta_i}\sin\left(\frac{\pi\Delta nd}{\lambda\cos\theta_i}\right)\cos\left(\frac{\pi\Delta nd}{\lambda\cos\theta_i}\right), \quad (2)$$

where η_{TE} is the DE for the transverse electric field, d is the grating thickness, Δn is the refractive index modulation, λ is the reduced wavelength, and θ_i is the incident wavelength. Figure 1 shows how the angular bandwidth of an example system changes based on the thickness of the holographic material.

Using this method, it is possible to accomplish beam steering that takes advantage of the low cost, form-factor, energy efficiency, and refresh rate of non-mechanical systems without being restricted to a narrow angular range. Figure 2 shows a schematic of the system and its final implementation in the demonstrator.

2. MATERIALS AND METHODS

This angular amplification system is composed of two distinct elements: a multiplexed grating that can direct the beam across 2π sr, which is recorded in a thick holographic recording medium to achieve high angular selectivity, and a shell hologram affixed to the surface of a hemispherical lens, whose purpose is to increase the diffraction angle from the initial multiplexed grating up to 4π sr while cancelling the focusing power of the hemisphere's surface.

A demonstration system was built with five distinct angle combinations, as shown in Table 1. Note that hologram 0 does not diffract the light from the multiplexed grating, but it does at the hemisphere surface. Due to the high angular selectivity of the gratings recorded in the multiplexed sample, light will

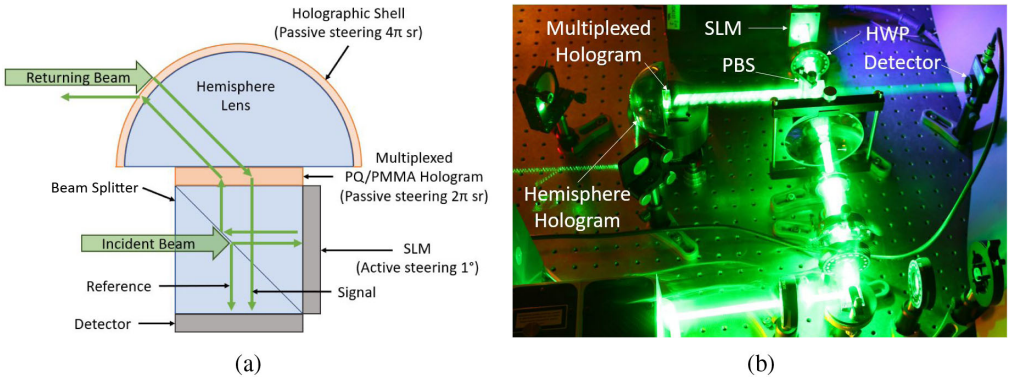

Fig. 2. Collimated light is shined through a beam splitter. Part of the light is redirected to the detector to serve as a reference signal, while most of it passes to the SLM. The SLM displays a diffraction pattern that steers the beam in the desired direction and reflects it back into the beam splitter. From the beam splitter, the light diffracted by the SLM is redirected to a high-angular-selectivity, multiplexed, volume hologram. This hologram diffracts the incident light over a 2π sr solid angle inside a hemispheric lens according to the incidence angle. On the convex surface of the hemispheric lens, HOEs are recorded to diffract light at an even broader angle and counteract the optical power of the hemispheric surface. The returning light follows a similar path through the holographic shell, hemispheric lens, and multiplexed hologram to arrive at the detector. (a) Theoretical layout of beam-steering system. (b) Real layout of beam-steering system.

Table 1. System Diffraction Angles[a]

Grating #	Incident Angle	Diffracted Angle (Multiplexed)	Diffracted Angle (Hemisphere)
0	0°	0°	20°
1	0.25°	20°	45°
2	0.5°	40°	90°
3	0.75°	60°	135°
4	1.0°	80°	150°

[a] Light with a given angle of incidence is diffracted by the multiplexed sample into the angle described. From there, it propagates to the hemisphere surface and is diffracted to the final angle.

not be diffracted by the multiplexed hologram, except at very specific angles. Hologram 0 demonstrates that even the light that is not diffracted by the volume hologram can be diffracted at the hemisphere surface for further beam-steering purposes.

A. Multiplexed Injection

The multiplexed injection hologram is designed to diffract a number of incident beams with relatively small inter-beam angles ($<1°$), such that the diffracted inter-beam angle becomes much larger ($\approx 90°$).

The multiplexed hologram was recorded in a holographic photopolymer called phenanthrene quinone doped polymethyl methacrylate (PQ/PMMA). This material was chosen because the material properties are well understood [17–24]. One characteristic of PQ/PMMA that is useful for recording these gratings with strong angular selectivity is that the thickness can be customized through the fabrication process to achieve the desired angular bandwidth of the encoded gratings. Additionally, the high-refractive-index modulation of the PQ/PMMA when recording holographic gratings is well suited to multiplexed recording [18]. Furthermore, the material demonstrates negligible shrinkage during the curing process, which means that recorded gratings will not change their slant angle or grating spacing after recording [17,18]. If the material did demonstrate shrinkage, the incidence angles of the beams used for recording would need to be chosen to accommodate the changing k-vector of the recorded grating.

PQ/PMMA samples were prepared in the manner described by Luo *et al.* in their work characterizing PQ/PMMA for holographic recording [25]. A recording geometry like that shown in Fig. 3(a) was assembled to record four distinct gratings with the reference beams near normal incidence and the object beams changing their incidence angle from 20° to 80° for a multiplexed, thick volume hologram. The beams are turned on sequentially, in pairs. Prisms are coupled to the front of the photosensitive sample to allow for injection of reference beams near normal incidence and object beams beyond the critical angle. An out-coupling prism prevents light from reflecting back within the material and creating secondary holograms.

B. Hemispheric Lens

The light diffracted by the PQ/PMMA sample can cover up to a 2π sr solid angle. Coupling this light into a hemispheric lens and applying holograms along the surface of that lens allows for that 2π sr solid angle to be expanded up to 4π sr. This was achieved by coating a hemispheric lens with discrete holographic optical elements (HOEs), which counteract the focusing effect of the convex surface and diffract the beam beyond its original propagation angle. Figure 4 shows the recording configuration selected to create these HOEs. A diverging beam whose source point is at the focal point of the hemisphere acts as the reference beam for recording these HOEs, while a collimated beam coming from the desired diffraction direction acts as the object beam.

Appropriate hologram recording geometries were modeled in Zemax OpticStudio to calculate the source point location of the reference beam for collimated diffraction from the hemisphere surface. Figure 5 shows collimated light incident at each hologram position and a collimated beam being diffracted by the hologram on the hemisphere surface.

3. RESULTS

A multiplexed grating was successfully recorded while minimizing signal crosstalk between the four different observation positions. Figure 6 shows the measured relative intensity values at four observation positions—20°, 40°, 60°, and 80°—when the incidence angle is varied from 0° to 1.25°. Readers will notice that the angles of peak diffracted intensity, as shown in Fig. 6, are different from those proposed in Table 1. This is due to a combination of the wedge angle from polishing the substrate and the slight angle introduced when using refractive-index-matching oil to couple the PQ/PMMA substrate to the hemisphere surface. This slight misalignment does not prevent

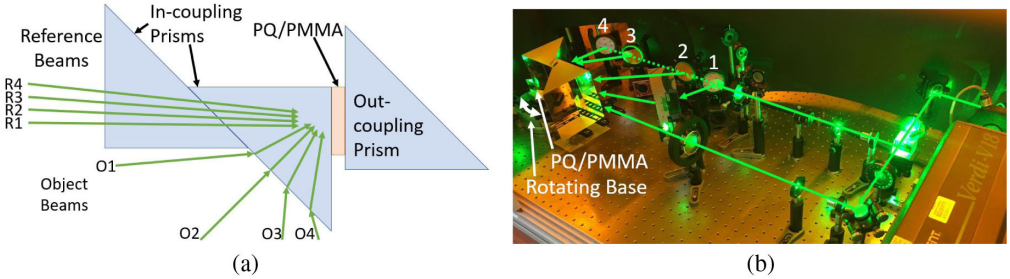

(a) (b)

Fig. 3. Recording configuration for multiplexed injection hologram. Gratings are recorded into the material with 10 s dark-delay time between exposures. (a) Recording configuration for multiplexed injection recording. All beams are shown at once, but each grating was recorded individually. (b) Real table layout for the multiplexed injection recording. Between recordings, the rotation stage was turned by 0.375° and the mirrors were removed, in order.

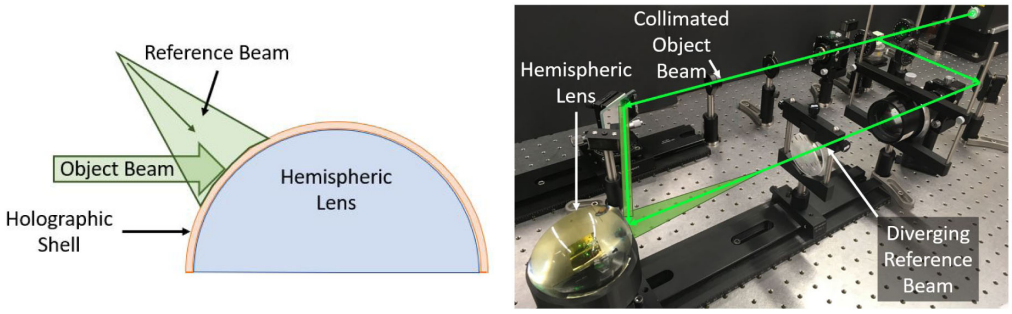

(a) (b)

Fig. 4. Holograms are recorded on the hemisphere surface with a diverging source beam and a collimated beam incident at the desired diffraction angle. The reference beam is a diverging beam that propagates toward the hemisphere surface where the focal point is the same distance as a collimated beam exiting the hemispheric lens. The object beam is collimated and propagates from the desired diffraction direction. (a) Theoretical setup for shell hologram recording. (b) Real setup for shell hologram recording.

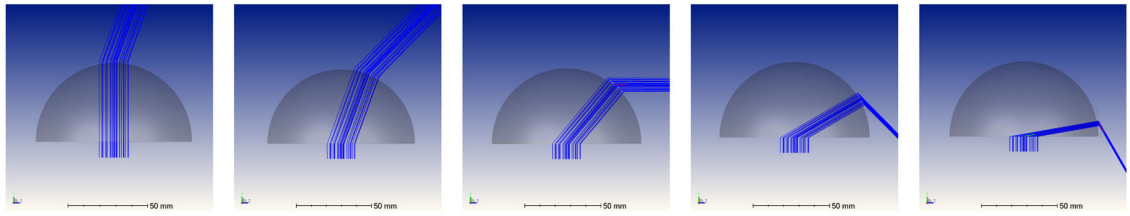

(a) (b) (c) (d) (e)

Fig. 5. Holograms recorded with the geometry shown in Fig. 4 will diffract collimated light from the hemisphere surface. (a) 0° to 20°. (b) 20° to 45°. (c) 40° to 90°. (d) 60° to 135°. (e) 80° to 150°.

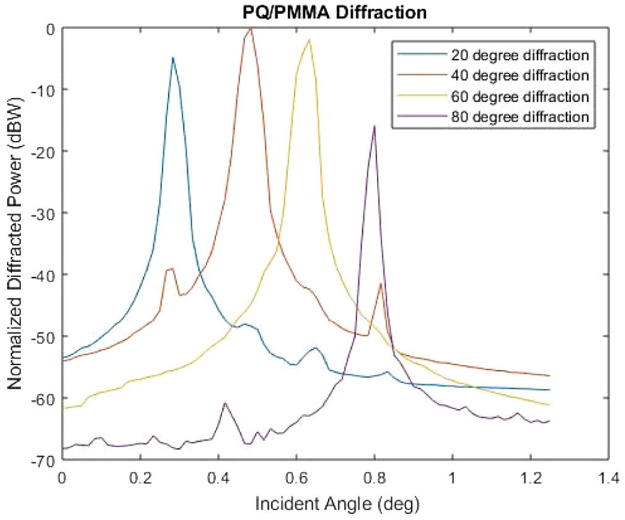

Fig. 6. Relative intensity values for multiplexed hologram at 20°, 40°, 60°, and 80° observation angles.

the system from demonstrating the angular selectivity and diffraction angle multiplication that was the intended result of this research, so the diffracted beams were measured "as is."

Kogelnik's CWT calculates an effective thickness and refractive index modulation for each of the gratings recorded in the multiplexed sample. Figure 7 shows the CWT curves overlaid on the DE curves, and Table 2 supplies the thickness and refractive index modulation parameters.

The intensity at the final diffraction angles (45°, 90°, 135°, 150°) were also measured after the light had propagated through the multiplexed hologram and the hemispheric shell. Figure 8 shows the observed intensities as a function of incident angle. Readers will notice that grating 0, which is discussed in Table 1, is not included in Fig. 8. This is because at every incidence angle on the multiplexed grating aside from those demonstrating high DE, light passes to grating 0 and is diffracted at 20°. In other words, the leakage from gratings 1 to 4 prevents the 0° from being used in this experiment. As more gratings are recorded into the multiplexed hologram, the leakage will decrease, and grating 0 can be used for beam steering.

Note that there is relatively less light in the 45° beam compared to the 90° beam in Fig. 8 than between the 20° and the 40° beam in Fig. 6. This is because the DE of successive elements must be considered. Table 3 shows the power budget for this demonstrator system.

After each individual component was tested, the entire system was assembled to demonstrate its feasibility with a lidar-type time-of-flight (TOF) measurement. Figure 2(b) shows the final system layout, which is based on the design in Fig. 2(a).

Light from a pulsed laser (6 ns pulse width) is expanded and passed through a polarizing beam splitter (PBS), which sends most of the light to the SLM, while a low-power reflection is used as a reference signal and sent directly to the detector. The beam incident on the SLM is double-passed through a half-wave plate (HWP), which rotates the polarization state 90° so that it is reflected from the plane bisecting the PBS and exits to the beam-steering setup. Light is diffracted by the multiplexed hologram to one of the hemispheric shell holograms. After the light

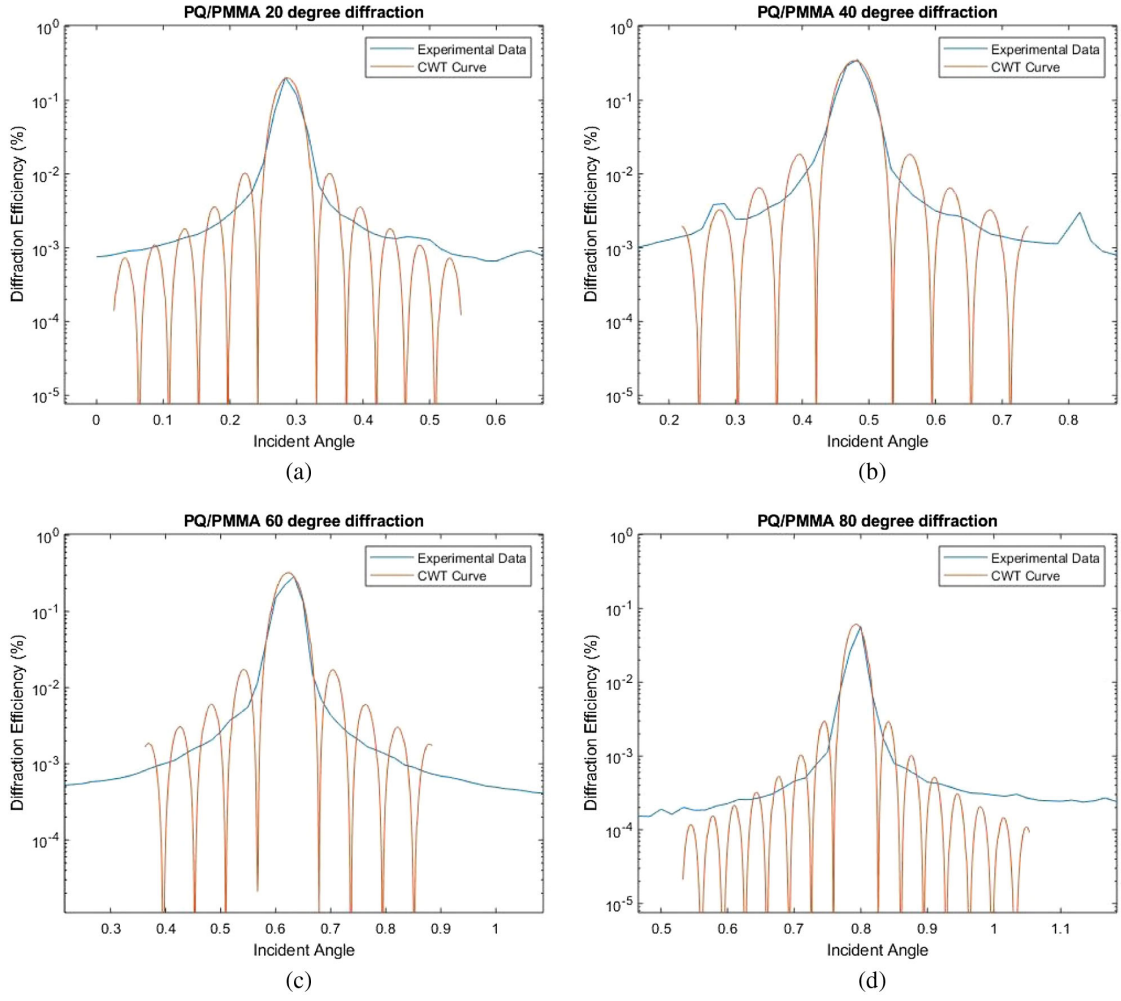

Fig. 7. CWT curve fitting of observed DE from multiplexed PQ/PMMA. (a) Grating 1 curve fitting. (b) Grating 2 curve fitting. (c) Grating 3 curve fitting. (d) Grating 4 curve fitting.

Table 2. Effective Grating Thickness and Refractive Index Modulation of Each Multiplexed Grating in the Thick Volume HOE

Grating #	Thickness (μm)	Δn
1	1900	3.9e-5
2	625	1.3e-4
3	310	1.7e-4
4	160	4.6e-5

has passed through the hemispheric shell holograms, it interacts with a HWP before it propagates a long distance. At the end of the path, the beam is retro-reflected back along the same path to the hemisphere. Interactions with the shell holograms and the multiplexed hologram diffract the returned beam back to the PBS. Because the beam has double-passed through the HWP, its polarization is again rotated 90° so that it passes through the PBS to the detector.

A high-speed silicon photodetector connected to a 3 GHz oscilloscope was used to measure the signal. Figure 9 shows the trace of the difference between the system with and without the signal beam.

The measured time difference between the reference peak and the TOF signal was 31.4 ± 1 ns, and the total path length difference between the two arms of the beam-steering arm was

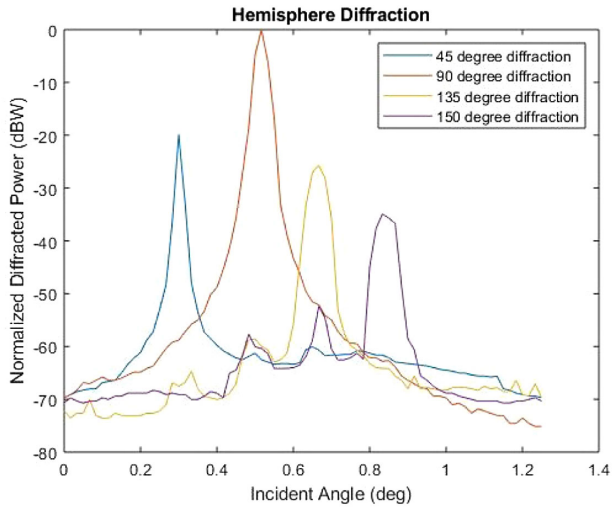

Fig. 8. Relative DE values for light diffracted by the multiplexed hologram and hemispheric shell holograms. Observation angles are 45°, 90°, 135°, and 150°.

Table 3. Power Budget for Demonstrator[a]

Element	DE	Discussion
SLM	37.3% at to ±0.381° 92% at 0°	Effective DE follows a $\mathrm{sinc}^2(1/N)$ response to the number of pixels (N) in one period of the blazed grating
Multiplexed grating 1	20.6%	
Multiplexed grating 2	35.7%	DE depends on grating thickness
Multiplexed grating 3	28.7%	and refractive index modulation
Multiplexed grating 4	5.8%	
Hemisphere grating 1	6.6%	DE depends on recorded efficiency
Hemisphere grating 2	37.0%	and agreement between design angle
Hemisphere grating 3	2.4%	and diffraction angle
Hemisphere grating 4	4.1%	from multiplexed grating

[a] DE of multiplexed grating combines with DE of hemisphere grating to determine overall efficiency of the system.

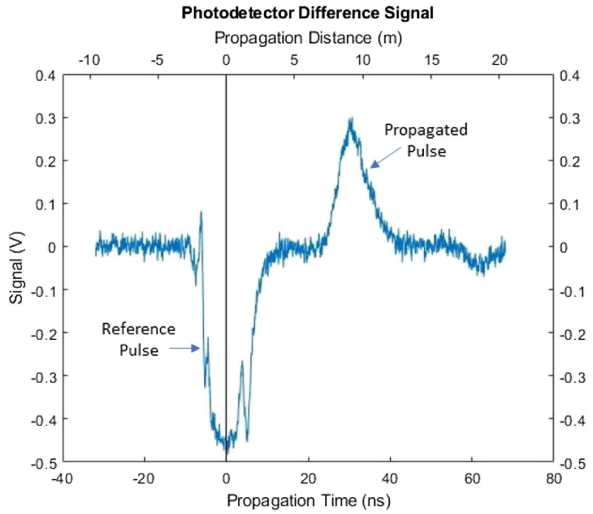

Fig. 9. Taking the difference between the detector signal with and without the beam-steering arm blocked shows that the return signal from the beam-steering system is detected 31.4 ns after the reference pulse.

measured to be 9.8 ± 0.1 m, which corresponds to a flight time of 32.6 ± 0.4 ns. This agreement between the measured and theoretical values demonstrates that this holographic, non-mechanical, beam-steering system works and, with continued refinement, will be a viable tool for use in lidar and other remote-sensing applications.

4. DISCUSSION AND CONCLUSION

Successive diffractive elements are combined to demonstrate a non-mechanical beam-steering method that can achieve a theoretical maximum of 4π sr redirection for lidar applications. This will aid in the design and implementation of systems that perform omni-directional scans of their environment. Commercial realization of this technology will require continued refinement of the hologram recording process to eliminate aberrations from the hemispheric lens, as well as a specialized application process to easily and uniformly affix a holographic film to the convex surface. Commercial implementation of this process will also require changing the design wavelength of the system. While the demonstrator discussed here is designed to work at 532 nm, lidar applications use 1.5 μm.

Future research efforts will seek to increase the angular selectivity and maximum DE of each recorded grating in the multiplexed hologram by increasing the exposure energy. Improving these parameters can be achieved by increasing the effective grating thickness and the refractive index modulation within the hologram. By making these adjustments, the multiplexed hologram will also be able to support a greatly increased number of gratings for higher-precision beam steering. The maximum number of gratings that can be multiplexed into a system is determined by the material thickness and maximum refractive index modulation. Diffraction efficiency of a thick volume holographic grating is given by Eq. (3) [15]:

$$\eta = \sin \frac{\pi \cdot \delta n \cdot d^2}{\lambda \cdot \cos \theta_0}, \tag{3}$$

where δn is the refractive index modulation within the material volume, d is the grating thickness, λ is the wavelength, and θ_0 is the incidence angle. As more gratings are multiplexed into the same material sample, the maximum refractive index modulation is split among more and more gratings ($\delta n = \delta n_{\max}/N$). This will decrease the efficiency of the recorded gratings unless some other parameter in Eq. (3) adjusts to compensate. The simplest and most effective parameter to change is the thickness (d), which has the added benefit of increasing the angular selectivity of the recorded grating. In this way, the DE of multiplexed gratings recorded in the medium can be maintained, even as the number of gratings is increased [see Eq. (2)].

As it has been demonstrated that thousands of holograms can be multiplexed in a thick volume hologram for purposes of data storage [26], it is also possible to record a similar number for purposes of beam steering, provided the appropriate material parameters.

Funding. National Science Foundation (1640329); University of Arizona (TRIF Link Funding).

Acknowledgment. The authors would like to thank Dr. Ray Kostuk and his students Jianbo Zhao, Sam Tan, and Ben Chrysler for their help with the PQ/PMMA sample preparation. They would also like to thank John Brownlee for his detailed notes on the PQ/PMMA sample preparation process. James Nekoliczak contributed to the hologram recording process. Additional thanks are due to Dawson Baker for his work polishing the PQ/PMMA sample for effective outcoupling. Lastly, the authors would like to acknowledge Dr. Yuzuru Takashima and his student Brandon Hellman for their advice on setting up a TOF measurement system.

Disclosures. The authors declare that there are no conflicts of interest related to this paper.

REFERENCES

1. I. Maksymova, C. Steger, and N. Druml, "Review of lidar sensor data acquisition and compression for automotive applications," in *Proceedings of Eurosensors* (2018).
2. B. Smith, B. Hellman, A. Gin, A. Espinoza, and Y. Takashima, "Single chip lidar with discrete beam steering by digital micromirror device," Opt. Express **25**, 14732–14745 (2017).
3. B. Kim and S. Gibson, "Adaptive control of a tilt mirror for laser beam steering," in *Proceedings of the 2004 American Control Conference* (2004), Vol. **4**, pp. 3417–3421.
4. C. Niclass, K. Ito, M. Soga, H. Matsubara, I. Aoyagi, S. Kato, and M. Kagami, "Design and characterization of a 256x64-pixel single-photon imager in CMOS for a MEMS-based laser scanning time-of-flight sensor," Opt. Express **20**, 11863–11881 (2012).
5. A. R. Cho, A. Han, S. Ju, H. Jeong, J.-H. Park, I. Kim, J.-U. Bu, and C.-H. Ji, "Electromagnetic biaxial microscanner with mechanical amplification at resonance," Opt. Express **23**, 16792–16802 (2015).
6. R. Moss, P. Yuan, X. Bai, E. Quesada, R. Sudharsanan, B. L. Stann, J. F. Dammann, M. M. Giza, and W. B. Lawler, "Low-cost compact MEMS scanning ladar system for robotic applications," Proc. SPIE **8379**, 837903 (2012).
7. A. Kasturi, V. Milanovic, B. H. Atwood, and J. Yang, "UAV-borne lidar with MEMS mirror-based scanning capability," Proc. SPIE **9832**, 98320M (2016).
8. V. Milanović, A. Kasturi, J. Yang, and F. Hu, "Closed-loop control of gimbal-less MEMS mirrors for increased bandwidth in lidar applications," Proc. SPIE **10191**, 101910N (2017).
9. J. Rodriguez, B. Smith, B. Hellman, A. Gin, A. Espinoza, and Y. Takashima, "Multi-beam and single-chip lidar with discrete beam steering by digital micromirror device," Proc. SPIE **10526**, 105260U (2018).
10. P.-A. Blanche, C. Bigler, C. Draper, J. McDonald, and K. Sarma, "Holography for automotive applications: from HUD to lidar," Proc. SPIE **10757**, 107570B (2018).
11. G. Chen, B. Hellman, J. Rodriguez, B. Smith, A. Gin, and Y. Takashima, "Light recycling beam steering on a DMD lidar," Proc. SPIE **10757**, 107570G (2018).
12. D. M. Benton, "Non-mechanical beam steering: ways and means," Proc. SPIE **10797**, 107970H (2018).
13. Q. Niu, C. Wang, H. Shi, L. Li, and D. Wang, "Development status of optical phased array beam steering technology," Proc. SPIE **11052**, 110521P (2019).
14. W. H. Bragg and W. L. Bragg, "The reflection of x-rays by crystals," Proc. R. Soc. London Ser. A **88**, 428–438 (1913).
15. H. Kogelnik, "Coupled wave theory for thick hologram gratings," Bell Syst. Tech. J. **48**, 2909–2947 (1969).
16. P. Zhu, X. Liu, and Z. Xu, "Color holography using the angular selectivity of volume recording media," Appl. Opt. **34**, 842–845 (1995).
17. G. J. Steckman, I. Solomatine, G. Zhou, and D. Psaltis, "Characterization of phenanthrenequinone-doped poly(methyl methacrylate) for holographic memory," Opt. Lett. **23**, 1310–1312 (1998).
18. S. H. Lin, K. Y. Hsu, W.-Z. Chen, and W. T. Whang, "Phenanthrenequinone-doped poly(methyl methacrylate) photopolymer bulk for volume holographic data storage," Opt. Lett. **25**, 451–453 (2000).
19. O. Beyer, I. Nee, F. Havermeyer, and K. Buse, "Holographic recording of Bragg gratings for wavelength division multiplexing in doped and partially polymerized poly(methyl methacrylate)," Appl. Opt. **42**, 30–37 (2003).
20. E. Tolstik, O. Kashin, A. Matusevich, V. Matusevich, R. Kowarschik, Y. I. Matusevich, and L. P. Krul, "Non-local response in glass-like polymer storage materials based on poly (methylmethacrylate) with distributed phenanthrenequinone," Opt. Express **16**, 11253–11258 (2008).
21. E. Tolstik, A. Winkler, V. Matusevich, R. Kowarschik, U. V. Mahilny, D. N. Marmysh, Y. I. Matusevich, and L. P. Krul, "PMMA-PQ photopolymers for head-up-displays," IEEE Photon. Technol. Lett. **21**, 784–786 (2009).
22. J. M. Castro, E. de Leon, J. K. Barton, and R. K. Kostuk, "Analysis of diffracted image patterns from volume holographic imaging systems and applications to image processing," Appl. Opt. **50**, 170–176 (2011).
23. Y. Qi, H. Li, E. Tolstik, J. Guo, M. R. Gleeson, V. Matusevich, R. Kowarschik, and J. T. Sheridan, "Study of PMMA-PQ photopolymer. Part 1: theoretical modeling," J. Opt. Soc. Am. B **30**, 3298–3307 (2013).
24. Y.-F. Chen, J.-H. Lin, S. H. Lin, K. Y. Hsu, and W.-T. Whang, "PQ:DMNA/PMMA photopolymer having amazing volume holographic recording at wavelength of insignificant absorption," Opt. Lett. **38**, 2056–2058 (2013).
25. Y. Luo, P. J. Gelsinger, J. K. Barton, G. Barbastathis, and R. K. Kostuk, "Optimization of multiplexed holographic gratings in PMMA-PQ for spectral-spatial imaging filters," Opt. Lett. **33**, 566–568 (2008).
26. L. Hesselink, S. S. Orlov, and M. C. Bashaw, "Holographic data storage systems," Proc. IEEE **92**, 1231–1280 (2004).